This article was published in Journal of Chemical and Engineering Data, 60(12), 3776-3791, 2015
http://dx.doi.org/10.1021/acs.jced.5b00708

Description and Test of a New Multilayer Thin Film Vapor Deposition Apparatus for Organic Semiconductor Materials

José C. S. Costa,*[,†,‡] Rui M. Rocha,[§] Inês C. M. Vaz,[†] Manuel C. Torres,[†] Adélio Mendes,[‡] and Luís M. N. B. F. Santos[†]

[†]CIQ – Centro de Investigação em Química, Departamento de Química e Bioquímica, Faculdade de Ciências da Universidade do Porto, Rua do Campo Alegre, 687, P-4169-007 Porto, Portugal

[‡]LEPABE – Laboratory for Process Engineering, Environment, Biotechnology and Energy, Faculdade de Engenharia, Universidade do Porto, Rua Dr. Roberto Frias, P-4200-465 Porto, Portugal

[§]CEMUP – Centro de Materiais da Universidade do Porto, Rua do Campo Alegre, 823, P-4150-180 Porto, Portugal

ABSTRACT

In this work the description, test, and performance of a new vacuum apparatus for thin film vapor deposition (ThinFilmVD) of organic semiconductor materials are presented. The apparatus is able to fabricate single, multilayer/composites, or hybrid thin films using four independent, organic or inorganic, vapor deposition sources (Knudsen cells type), and the vapor mass flow is condensed onto a substrate surface (temperature regulated). The same apparatus could be also used to measure vapor pressures according to the Knudsen effusion methodology. Vapor pressures and thermodynamic properties of sublimation measured by Knudsen effusion of some reference organic materials (benzoic acid, anthracene, triphenylene, benzanthrone, 1,3,5-triphenylbenzene, perylene) were used to evaluate and test the performance of the apparatus. Moreover, nanostructures of thin films and composite materials of relevant charge transport and electroluminescent materials were deposited onto an indium−tin oxide (ITO) surface, and the morphology and thin film thickness were evaluated by scanning electron microscopy (SEM), exploring the effect of different mass flow rates and deposition time. The new physical vapor deposition apparatus based in four Knudsen effusion cells with an accurate mass flow control was designed to assemble well-defined (composition, morphology, thickness) thin films of organic semiconductors based on their volatility. The described apparatus presents a high versatility to the fabrication of single/multilayer thin films, as- grown crystals, and hybrid micro- and nanostructured materials.

INTRODUCTION

Vapor deposition is one of the most used and efficient methods to fabricate thin films onto a solid surface. The layers range from a thickness of one atom up to millimeters, forming single thin films, bilayer, trilayer, or multilayer composites as well as hybrid thin film materials. There are two main vapor deposition processes: chemical vapor deposition (CVD) and physical vapor deposition (PVD). When the vapor source is a chemical vapor precursor, the process is called CVD, and

it has several variants: low-pressure chemical vapor deposition (LPCVD),[7,8] plasma-enhanced CVD (PECVD),[9,10] and plasma-assisted CVD (PACVD).[11,12] CVD is often used in the semiconductor industry to produce organic and inorganic thin films.[13,14] In PVD, the vapor source is a solid or liquid material, and this method implicates only physical processes such as high-temperature vacuum sublimation/vaporization with consequent condensation onto a substrate surface. There are several variants of PVD: cathodic arc deposition,[15,16] electron beam PVD,[17,18] evaporative deposition,[19,20] pulsed layer deposition,[21,22] and sputter deposition.[23,24] PVD techniques are more environmentally friendly than traditional coating methods with several applications under the scientific and industrial points of view. In fact, thin films produced by PVD are developed and applied in electrical and semiconductor manufactories, for instance in organic electronics and optoelectronics (OLEDs, OPVs, OFETs), and used for energy conservation and/or generation.[25−30] Herein, we present a high vacuum thin film deposition apparatus, ThinFilmVD, for physical vapor deposition of organic semiconductor materials (OSCs) with electronic applications. The thin film deposition is controlled by a mass flow in equilibrium conditions generated by four independent Knudsen cells (vapor deposition sources). The rate of the deposition is defined and regulated by the vapor pressure of the organic compounds at the effusion temperature and the substrate surface distance to the effusion cell orifice. Hence, the system presented herein allows accurate vapor pressure measurements as well as a high versatility to the deposition of single thin films, as-grown crystals, composites, and hybrid micro- and nanostructured materials.

Knudsen effusion based methods are the most widely used for measuring the vapor pressures of solid and liquid organic compounds for pressures lower than 1 Pa.[31−33] At the temperature T, the mass m of the sample sublimed/vaporized from the effusion cell, during the time period t, is related to the vapor pressure of the compound by eq 1.

$$p = (m/A_0 w_0 t)(2\pi RT/M)^{1/2} \quad (1)$$

where M is the molar mass of the effusion vapor, R is the gas constant, A_0 is the area of the effusion orifice, and w_0 is the transmission probability factor which is usually calculated by means of Clausing (2) or Dushman (3) equations, where l is the length of the effusion orifice and r its radius:[34−36]

$$w_0 = [1 + (l/2r)]^{-1} \quad (2)$$

$$w_0 = [1 + (3l/8r)]^{-1} \quad (3)$$

The quality and performance of the system presented herein were evaluated based on the experimental measurements of the vapor pressures and derived thermodynamic parameters of sublimation of some reference materials: benzoic acid, anthracene, triphenylene, benzanthrone, 1,3,5-triphenylbenzene, and perylene. Thin films, composites, and hybrid materials were produced onto glass substrates with previously deposited ITO thin film by vacuum deposition of some relevant tris-8-hydroxyquinolinatos, triphenylamine derivatives, and oligoacenes. The thin film morphology of organic semi-conductors were evaluated by scanning electronic microscopy (SEM).

The system can be considered a very "clean" and "user- friendly" apparatus, due to the absence of very greased junctions and overall easy handling of the different components, which enables a quick

assembling and disassembling of the sublimation/vaporization chamber components at the beginning and at the end of each effusion/thin film deposition experiment

APPARATUS AND EXPERIMENTAL PROCEDURE

Overview

The ThinFilmVD apparatus presented herein is constituted by four independent ovens allowing the sequential or simultaneous effusion of four different samples, an efficient vacuum pumping system ($p \approx 10^{-4}$ Pa), an independent and precise, proportional integrative and differential (PID) temperature control of the Knudsen cells that are maintained inside independently copper blocks (ovens), air based fast cooling of each oven, as well as a precise temperature control of the deposition substrate surface by means of refrigerated bath and a PID temperature control metallic platform. The combination of the vapor pressure of each compound at the respective oven temperature and the distance to the deposition substrate surface is used to define the mass flow density. The film deposition rate (related with mass flow density at the substrate surface) and deposition time is used to control the film thickness and morphology. Based on the independent ovens, single thin films, bilayers, composites, as well as, hybrid films can be produced from the sublimation/ vaporization of each material. A schematic representation of the overall ThinFilmVD apparatus is presented in Figure 1. Additional images and schematic drawings and details of the apparatus are presented as Supporting Information (SI).

Vacuum Chamber and Pumping System

The stainless steel vacuum chamber is divided in two main parts, bottom and top (see details in Supporting Information). The bottom contains the insets (NW50) for each oven and the top the connection between the chamber and the vacuum pumping system and includes the substrate support system. In order to avoid the contamination of the turbomolecular pump, a metallic trap with liquid nitrogen is located between the vacuum system and the top of the chamber. The top and bottom are connected by a mechanical hinge system (with VITON O-ring) that allows an easy handling and operation of the vacuum chamber. The top of the chamber contains connections for gas inlet, inlet/outlet of the circulation cooling fluid, the Pt100, heater cables vacuum insert connectors to the temperature control of the deposition substrate surface, and the thickness monitor quartz crystal microbalance holder. The vacuum pumping system is constituted by a turbomolecular pump Adixen ATP80/ACT200TH/ACS2000 and a rotary vane pump Pascal 2005 SD. The chamber pressure is measured with a wide range vacuum transducer Adixen ACC2009. The pumping system is connected to the chamber by a flexible hose metal. The vacuum system allows the decreasing of the pressure in the chamber until 10^{-4} Pa.

Ovens

The ThinFilmVD comprises four independent ovens for the selective effusion of each material. Each oven was built in copper (cylindrical block of 50 mm long and 40 mm diameter), comprises a U shape air cooling stainless steel tube (6 mm diameter), an electric heater of 100 W and a Pt100 temperature sensor, which allows a temperature control with a temperature stability better than ± 0.05 K until 700 K. Each oven was perforated according to the Knudsen cell dimensions, which are screwed directly in the oven (copper block) in order to ensure a good vacuum thermal contact. All ovens present an individual and automatic air cooling system. A schematic representation of the ovens

showing the respective position inside the chamber is presented in Figure 2

Effusion Cells

The effusion cells were fully built in stainless steel and set up to each oven by means of a screwing system. The cells are divided in three main parts: the cell lid, the cell body, and the disk with an orifice (Figure 3). The lid and the body are attached by means of a fine-pitched screw thread. A thin stainless steel (AISI 316) disks (thickness of 0.32 mm or 0.050 mm and orifices with different diameters: 1.0 mm; 1.2 mm; 2.0 mm; 3.0 mm) are mounted on each cell according to the scheme presented in Figure 3. The orifice area of each stainless steel disk was measured by means of optic microscopy with an uncertainty better than 0.5 %, and the results are presented as SI. The dimensions of the closed cells are 15.7 mm diameter and 20 mm height. Although the stainless steel presents lower thermal conductivity than aluminum (frequently used in Knudsen cells), this alloy has higher thermal resistance, resistance to the corrosion, as well as high durability. Due to the low volatility of organic semiconductors, the ThinFilmVD needs to operate at high temperatures, and stainless steel (AISI 316) was found to be the best available alloy.

Prior to each experiment, the Knudsen cells are typically cleaned with several solvents with different polarities (deionized water, ethanol, acetone, and dichloromethane) and after heated at high temperature (600 K) in high vacuum conditions, typically during 30 min.

Substrates Support and Thickness Monitor

The thin film deposition substrates support, stainless steel (AISI 316) disk (80 mm × 20 mm), is screwed to a refrigerated copper tube that is mechanical adjusted to define the distance of the substrates support to the effusion orifice. The temperature of substrate is measured by Pt100 that is also used for the PID controller using a 100 W electric heater and a refrigerated liquid bath (Huber Minichiller, typically at 265 K). A cooled quartz crystal microbalance Inficon, model CDS-BOF37 Cool Drawer (located at the same distance from the orifice), and STM-2 Rate thickness monitor are used for the real time thin film thickness evaluation and control.

Auxiliar Instrumentation Box

The instrumentation box comprises five PID temperature controllers Omron, model E5CC-QX3A5M-000, with universal entry, exit to solid state relay (SSR), Pt100 temperature sensors, and additional exits, which are used in the automatic cooling system of the ovens. Each controller is connected to a SSR G3PE-225B DC12-24 of 25A/100-240VAC with a heat sink (see details in Supporting Information). The alarm system and control of the cooling system with compressed air operates at low voltage (24VAC). The automatic cooling system of the ovens uses electro- magnetic solenoid valves of 24VAC that drives the air cooling flow through the system. As evidenced in Figure 1, the system presents manual switches that are used to drive each oven cooling system as well as to drive/interrupt the electric heating in each individual oven. The set point temperature of each oven is programmed independently by each controller E5CC. The PID temperature controllers (PID parameters) were previously optimized for the better isothermal temperature control and small overshooting. One of the controller alarms was programed to actuate (on the cooling system) for temperatures above 1 K the set point temperature.

Temperature Measurement and Control

All of the Pt100 sensors were calibrated by comparison against a platinum resistance thermometer,

PTR100 (Fluke, Hart Scientific, model 5626), traceable to the National Institute of Standards and Technology (NIST) based on the ITS-90 temperature scale, with an uncertainty smaller than 0.002 K. For that purpose a refrigerated thermostatic oil bath was used, which allowed a calibration between 50 and 190 °C. The measurement of the oven temperature was carried out in real time using data acquisition switch unit multimeter, 61/2 digits, Agilent 34970A.

Measurement of Vapor Pressures

The Thin- FilmVD system is able for measuring vapor pressures by Knudsen effusion methodology,[32,33] and the following experimental procedure was followed (the numbers between brackets are referred to the Figure 1): initially, the vacuum chamber (1), metallic trap (9), substrates support system (5, 17), ovens (2), and respective Knudsen effusion cells should be carefully cleaned; after placing all components in the system, the vacuum chamber can be closed, and then the metallic trap is filled with liquid nitrogen, and the system is pressurized by the turbomolecular pump (11) during 30 min, by opening the vacuum valve (10); after the cleaning methodology, the system is despressurized with nitrogen, and the vacuum chamber can be opened; the Knudsen cells are retired from their respective ovens and placed in a desiccator during 60 min; the sample is compressed inside the cells by a brass piston in order to obtain a flat surface and to improve the thermal contact. The amount of sample used is the quantity necessary to obtain a disk of ≈ 5 mm height after the compression. The cells holding the sample are weighed on an analytical balance (Mettler Toledo, model H54, with a readability of 0.00001 g); the cells are then screwed in their respective ovens, and the temperature of each one is programmed as desired. After allowing for thermal stabilization of the Knudsen cells, the vacuum chamber is connected to the pumping system. When the pressure is lower than 1 Pa, the metallic trap is filled with liquid nitrogen, and the effusion time period is considered to start. In less than 1 min, after opening the gate valve, a pressure lower than 10^{-3} Pa is obtained. When the chosen effusion time period is over, the isolation valve is closed, and nitrogen is allowed to enter into the chamber, by opening the gas inlet valve (7). By decreasing the temperature of each oven, the individual cooling system of each oven automatically starts. After cooling to ambient temperature, the cells are carefully cleaned and weighed using the analytical balance.

Thin Film Deposition

The vapor pressure is a key parameter for thin film deposition with the system presented herein. The experimental procedure is identical to any classical Knudsen effusion experiment, but with the ThinFilmVD, the vapor effused from the Knudsen cells condenses on the surface of a substrate, and a thin film is formed. For achieving this goal, a desirable substrate is placed on the substrate support system, and the experimental procedure is the same as presented in Section 2.7. Before starting an experiment the substrates should be rigorously cleaned with two or more solvents in an ultrasonic bath and dried with and inert gas. Depending on the experimental methodology, single thin films, composites, as well as hybrid materials can be produced by low-pressure sublimation/vaporization. The substrate temperature is defined by the substrate support PID controller. For the formation of a single thin film onto the substrate surface, an intended organic semiconductor is placed in one or more Knudsen cells and sublimated/vaporized according to its vapor pressure (calculated by eq 1). The vapor pressure commands the mass flow effused from the cells. Nanostructured or non-nanostructured composites are produced by assembly of thin films by means of successive deposition of layers. In this case, different organic semiconductors are placed in the Knudsen cells and

sublimated/vaporized sequentially according to their volatility.

The temperature of each oven is programmed according to the volatility desirable for the compounds. The hybrid nanomaterials are produced by simultaneous sublimation/vaporization of different compounds. The effusion time, the vapor pressure of each compound, and the substrate temperature can be adjusted in order to modify the morphology and thickness of the films/composites.

Thin Film Morphology

In this work, thin films and composites of several OSCs were deposited onto a surface of indium tin oxide (ITO) coated glass, and their morphology was studied by high-resolution scanning electron microscopy with X-ray microanalysis and backscattered electron diffraction pattern analysis, with a FEI Quanta400FEG/EDAX Genesis X4M instrument at 15 kV in low-vacuum mode at the CEMUP (Centro de Materiais da Universidade do Porto). Topographic images were acquired using a secondary (SE) detector.

3. RESULTS AND DISCUSSION

Vapor Pressures and Thermodynamic Properties of Sublimation of Organic Materials.

In order to test the quality of the results obtained with the ThinFilmVD apparatus, the vapor pressures of the following six organic compounds were measured over temperature intervals of ca. 25 K: benzoic acid (CAS Number 65-85-0), anthracene (CAS Number 120- 12-7), triphenylene (CAS Number 217-59-4), benzanthrone (CAS Number 82-05-3), 1,3,5-triphenylbenzene (CAS Number 612-71-5), and perylene (CAS Number 198-55-0). The studied samples were previously purified by sublimation under reduced pressure, and GC analysis showed that the mass fraction purity was not less than 0.999 in all cases. The areas and transmission probability factors of the used effusion orifices in stainless steel disks of 0.32 mm thickness and the detailed experimental results obtained from each individual effusion cell are presented as SI. Very good results of vapor pressures calculated by using the Clausing transmission probability factor can be obtained (the deviations are lower than 0.1 Pa). However, due to the higher thickness of the orifices used, a new transmission factor was used. The w_O was obtained by comparison of the results obtained with the ThinFilmVD and experimental data recommended by Ribeiro da Silva and Santos et al. for benzoic acid, anthracene, triphenylene, benzanthrone, 1,3,5-triphenyl- benzene, and perylene. In all cases the following equation was derived: $w_0 = [1 + (3l/4r)]^{-1}$.

Tables 1, 2, 3, 4, 5, and 6 present the vapor pressures at several temperatures obtained using the ThinFilmVD apparatus for benzoic acid, anthracene, triphenylene, benzanthrone, 1,3,5-triphenylbenzene, and perylene, respectively. Depending on the sublimation temperature, the uncertainty of the vapor pressure is estimated to be as (2 to 5) % of the experimental value.

Table 7 presents, for each compound studied, the experimental results obtained of the four groups of effusion cells used (C1, C2, C3, C4) and for the global treatment of all of the (T, p) points obtained for each compound, the detailed parameters of the Clausius−Clapeyron eq (eq 4), together with the calculated standard deviations and the standard molar enthalpies of sublimation at the mean temperature ($\langle T \rangle$) of the experiments, $\Delta_s{}^g H^o{}_m$ ($\langle T \rangle$). The equilibrium pressure at this temperature, p ($\langle T \rangle$), and the entropies of sublimation at equilibrium conditions, $\Delta_s{}^g S_m$ ($\langle T \rangle$; $p\langle T \rangle$)), are also presented. The plots of $\ln p = f(1/T)$ for each compound studied are presented in Figures 4, 5, and 6. Plots obtained by other researchers are also depicted for comparison.[31,33,37−39]

The standard molar enthalpies of sublimation at the mean temperature of the sublimation experiments were derived for the compounds studied, using the integrated form of the Clausius–Clapeyron according to eq 4.

$$\ln(p/\mathrm{Pa}) = a - b[(1/T)/\mathrm{K}^{-1}] \qquad (4)$$

where a is a constant and b = $\Delta_s^g H^o_m(\langle T\rangle)/R$. The standard molar enthalpies of sublimation at the mean temperature, $\Delta_s^g H^o_m(\langle T\rangle)$, were determined by the parameter b, of the Clausius–Clapeyron equation, and the molar entropies of sublimation at the mean temperature and at the vapor pressure at the mean temperature, $\Delta_s^g S_m(\langle T\rangle; p\langle T\rangle))$, were calculated by eq 5.

$$\Delta_s^g S_m(\langle T\rangle, p(\langle T\rangle)) = \Delta_s^g H^o_m(\langle T\rangle)/\langle T\rangle \qquad (5)$$

The standard molar enthalpies of sublimation, at T = 298.15 K, $\Delta^g_s H^o_m$, were determined by eq 6.

$$\Delta_s^g H^o_m(T) = \Delta_s^g H^o_m(\langle T\rangle) + (T - \langle T\rangle)\cdot\Delta_s^g C^o_{p,m} \qquad (6)$$

The standard molar entropies of sublimation, at T = 298.15 K, $\Delta_s^g S^o_m$, were calculated using eq 7.

$$\Delta_s^g S^o_m(T) = \Delta_s^g S_m(\langle T\rangle, p(\langle T\rangle)) + \Delta_s^g C^o_{p,m}(T)\ln(T/\langle T\rangle) - R\ln(p^o/p(\langle T\rangle)) \qquad (7)$$

where $p^o = 10^5$ Pa. $\Delta_s^g C_p$ is the variation in molar heat capacity associated with sublimation process, obtained by a temperature adjustment using the difference between the heat capacities of the gas and solid phases, at T = 298.15 K, derived as $\Delta_s^g C^o_{p,m} = C^o_{p,m}(g) - C^o_{p,m}(s)$. Recommended values of $\Delta_s^g C^o_p$ = (−44.4, −27.0, −39.9, −29.0, −37.3, and −42.6) $J\cdot K^{-1}\cdot mol^{-1}$ were used for benzoic acid, anthracene, triphenylene, benzanthrone, 1,3,5-triphenylbenzene, and perylene, respectively.[31,33,40]

The standard molar Gibbs energies of sublimation were calculated through eq 8 where the parameters are referenced to T = 298.15 K.

$$\Delta_s^g G^o_m(T) = \Delta_s^g H^o_m(T) - T\cdot\Delta_s^g S^o_m(T) \qquad (8)$$

Table 8 lists the derived standard molar enthalpies, entropies, and Gibbs energies of sublimation, at T = 298.15 K, for the compounds studied.

As evidenced by Figures 4, 5, and 6, the dependence between vapor pressures and temperatures determined with the ThinFilmVD system for benzoic acid, anthracene, triphenylene, benzanthrone, 1,3,5-triphenylbenzene, and perylene is very consistent with the results obtained and recommended by other researchers. Analyzing these data, within the experimental error very concordant plots of ln p = f(1/T) were obtained with the four ovens and respective Knudsen

cells used. Based on those plots, thermodynamic properties of sublimation were derived for each compound and converted to T = 298.15 K by considering the heat capacity variation associated with the sublimation process. Considering the average of the thermodynamic parameters derived from the data obtained from each Knudsen cell (C1, C2, C3, C4), standard enthalpies, entropies, and Gibbs energies of sublimation were determined and compared with some selected literature data (Table 8). As evidenced, a high consistency between the results presented herein and the data recommended by other researchers were found. Therefore, the ThinFilmVD system is capable to measure vapor pressures of organic materials with high precision as well as to derive thermodynamic properties associated with the phase transition.

Thin Film Topography

Based on the precise knowledge of vapor pressure, thin films can be produced by vacuum sublimation onto desirable substrates. The fact that ThinFilmVD system can operate simultaneously with four independent ovens allows depositing thin films sequentially to produce composites or hybrid nanostructures. Herein, the topography of thin films of TDAB (hole transport material, CAS Number 126717-23-5), NPB (hole transport material, CAS Number 123847-85-8), *mer*-Gaq3 (electron transport material/electroluminescent, CAS Number 14642-34-3), *fac*- Inq3 (electron transport material/electroluminescent, CAS Number 14514-42-2), and rubrene (charge transport material, CAS Number 517-51-1) produced onto ITO coated glass is presented. Some molecular/supramolecular properties and important thermophysical properties of these compounds were previously explored in other works.[25,26,39] Before the deposition, all samples were purified by sublimation under reduced pressure. All compounds are organic semiconductor materials with important applications as thin films for organic electronics and optoelectronics.[25,26,39] The vapor pressures of these materials were determined previously and confirmed with the ThinFilmVD system (see details in SI). All details related to the deposition experiments are available as SI. Initially, a test (experiment 1) was made with TDAB that was sublimated from Knudsen cell C1 at $T \approx 505$ K ($p \approx 0.5$ Pa) with effusion/ deposition times of 15/30/45/60/90/120 min. For this experiment the distance between cell and substrate was fixed as h = 25 cm. In the experiment 2, TDAB was sublimated from Knudsen cells C2 and C4 with the same vapor pressure ($p \approx 0.5$ Pa) with effusion times of 30/60/90/180 min, and the distance between cells and substrate was decreased to h = 10 cm.

Figures 7 and 8 present the topographic images of the nanostructures of TDAB deposited onto the ITO surface by vacuum deposition using the ThinFilmVD. All of the images presented in this work were acquired by SEM and using a secondary electron detector.

According to Figures 7 and 8, the decreasing of the distance between the cells and the substrate and the use of more Knudsen cells contribute for a higher number of nanostructures of TDAB deposited onto the ITO surface. By using higher cell- substrate distances, the compound effused is mostly deposited on the walls of the deposition chamber. The use of more Knudsen cells corroborates for a higher quantity of material deposited on the substrate. Considering the nucleation and growth mechanisms of thin films,[56–62] due to the low condensation of material onto the ITO surface (Figure 7), the clusters deposited probably diffuse through the surface and most of them are desorbed because of the low number of neighbor clusters to promote interactions and favor the thin film/nanostructures growth. The decreasing of the distance between the ovens and substrate and by using more Knudsen cells (Figure 8) a higher number of clusters deposited is observed. Due to the structural and thermodynamic properties of TDAB, this compound condenses preferentially with an

crystalline structure, and the formation of a flat thin film is difficult.[25,63] According to the experimental conditions, the increasing of the effusion time (from 30 to 180 min) contributes for a gradual growth of the TDAB nanostructures. The use of higher effusion times is responsible by the increasing of nucleation/growth mechanisms of clusters. The affinity between substrate and clusters is an important property to consider for the thin film morphology and its occupancy rate on the surface. Herein all the depositions were performed onto the ITO surface. Additionally, the substrate temperature is a crucial property for the thin film deposition process, namely, for the thermal accommodation and formation of the clusters. The organic semiconductors usually present low volatility/high evaporation temperatures, and thus the difference between the temperatures of the vapor effused and the substrate (usually higher than 200 K) is enough for the easy formation and accommodation of clusters.[25,26,31,63] Nevertheless, small variations in the temperature of the surface can be enough for some modifications of the adhesion, growth, thickness, and morphology of the thin films.

As presented in the following results (experiment 3), the relation between the vapor pressure and the morphology of the nanostructures was studied. For that purpose, several sublimation temperatures ($T \approx 493/498/503/508$ K) were used, and an effusion time of 60 min was fixed (TDAB was sublimated from Knudsen cells C2 and C4). The other experimental conditions were maintained constant. Figure 9 presents the topographic images obtained.

As observed, the use of different mass flows (different vapor pressures/sublimation temperatures) contribute for the morphology and size of the TDAB nanostructures. Often, by maintaining the other experimental conditions, slight increments in the vapor pressure result in the formation of nanostructures with higher size. For a specific compound, the precise knowledge of the vapor pressure and its dependence with the temperature is relevant for the deposition of thin films by vacuum sublimation.

Figure 10 allows a comparison between the topographic images of TDAB and Gaq3 deposited onto the ITO surface by vacuum deposition using the ThinFilmVD (experiment 4). Both compounds were sublimated with the same vapor pressure ($p \approx 0.5$ Pa) with effusion times of 30 and 60 min (both compounds were sublimated from Knudsen cells C2 and C4).

According to the topography, the increasing of the effusion time (30 to 60 min) promotes the adhesion between clusters and the growth of the nanostructures. In the case of *mer*-Gaq3, a flat thin film with a thickness of ≈100 nm was produced. Doubling the effusion time, the thin film produced modified his flat morphology, and the thickness was incremented twice (≈ 200−250 nm). For TDAB, the morphology is similar to presented in previous figures. In contrast to verified for Gaq3, the size of the nanostructures was not significantly incremented with more effusion time; however, the number of nanostructures is higher with 60 min of deposition, and the surface of ITO with compound deposited was considerably increased. As evidenced by analyzing the topographical structures, some nanocrystals of TDAB and *mer*-Gaq3 seem to grow on the surface of their thin films. In most cases, thin films produced by vacuum deposition are more amorphous; however, the amorphicity of the nanostructures is quite dependent by the experimental conditions and highly related with the supra-molecular and thermodynamic properties of each material.

Figure 11 presents the topography of some amorphous thin films (rubrene, NPB, and *fac*-Inq3) deposited onto the ITO surface by vacuum deposition using the ThinFilmVD (experi- ment 5). Both compounds were sublimated from a Knudsen cell C2 with the same vapor pressure ($p \approx 0.5$ Pa) with effusion times of 30 and 60 min.

As illustrated, amorphous nanostructures of rubrene, NPB, and *fac*-Inq3 were produced from the sublimation of each material, and for all compounds a good adhesion between the thin film and the ITO surface seems to be obtained. As observed, the nanostructures were deposited preferentially on specific areas of the substrate (probably more rough) giving a deposition pattern that is highly dependent by the surface nature. For the rubrene, nanostructures with a size of ≈110 nm were produced by using 30 min of effusion, and their size was incremented to ≈190 nm with 60 min of deposition. The increasing of the deposition time was also responsible by a lower surface area occupied by the rubrene nanostructures due to the coalescence of the neighbor clusters. A similar conclusion can be observed from the morphological analysis of *fac*-Inq3 based thin films. Nanostructures with an average size of 120 and 180 nm were produced by using 30 and 60 min of effusion time, respectively. Contrary to verified with rubrene and *fac*- Inq3, the morphology of the NPB nanostructures was modified by using different deposition times. For this compound, nanostructures with a size of ≈150 nm were produced; however, the increasing of deposition time was responsible for relevant coalescence mechanisms that have changed the morphology of the thin films.

In addition to the deposition of monolayers, composite thin films of some OSCs can be produced by the combination of the four ovens of the ThinFilmVD system and according to the vapor pressure/sublimation temperature of each individual compound. Thus, Figure 12 presents the topography of composite thin films of rubrene, NPB, and *fac*-Inq3 deposited onto the ITO surface by vacuum deposition using the ThinFilmVD (experiment 6). The compounds were successively sublimated by Knudsen cell C2 with the same vapor pressure ($p \approx 0.5$ Pa) with effusion times of 30 and 60 min.

In this experiment, a NPB/Inq3, Inq3/NPB and NPB/ rubrene bilayers, a NPB/Inq3/NPB and NPB/rubrene/Inq3 trilayers, and a NPB/Inq3/NPB/Inq3 multilayer were deposited by using an ITO coated glass as substrate. All composites present nonsimilar morphology. The bilayers of NPB/Inq3 and Inq3/NPB present a distinct morphology due to the different interfaces between the thin films. For the first one, NPB was deposited onto the ITO surface, and Inq3 was deposited onto the previously deposited NPB. Distinctively, in the second structure, Inq3 was deposited onto the ITO, and NPB was deposited onto the Inq3 surface. An additional vacuum deposition of a desirable material on the surface of a previously deposited nanostructure contributes for increasing the adhesion with the surface and for the thin film growth as well as for the occupation of interstices and voids on the substrate surface. The deposition of three or more materials with different chemical nature leads to the formation of a flat composite (multilayer thin films) with high rate of surface occupation. As it can be observed by analyzing the results presented in this work the morphology of a composite material differs to the morphology of each thin film constituent of the multilayer.

This possibility to produce composite nanostructures based on the volatility of each constituent is one of the main advantages of the ThinFilmVD system. The deposition of most organic composite thin films is usually difficult with solution methods due to the low solubility of OSCs. Additionally, the deposition of a material by spin or dip coating methods on the surface of previously deposited thin films can implies the dissolution or creep of the first nanostructure. Nevertheless, physical vacuum deposition and solution coating methods can be used together for assembling nanostructured materials.

CONCLUSIONS

A thin film vacuum deposition system (ThinFilmVD) was built and tested for the deposition of thin films and composites of organic semiconductors. The system presented herein allows to measure with high precision the vapor pressure of a specific material by the Knudsen effusion methodology and relate this data with a thin film controlled deposition onto desirable substrates. One of the most advantages of the ThinFilmVD is the possibility of depositing sequentially or simultaneously thin films from the sublimation/vaporization of a material from four independent ovens. As presented for several organic systems with great importance for materials science and engineering, a thermodynamic evaluation of the crystal/solid stability of materials including accurate vapor pressure measurements are of great relevance for the manufacturing technology of thin films by vacuum deposition.

ASSOCIATED CONTENT

Supporting Information

The Supporting Information is available free of charge on the ACS Publications website at DOI: 10.1021/acs.jced.5b00708.

Schemes and figures related to the ThinFilmVD apparatus (Table S1−S2, Figures S1−S5), sublimation equilibrium results including vapor pressure determinations (Tables S3−S8), and the data for the thin films deposition and their morphological analysis (Tables S9− S14, Figures S6−S13) (PDF)

AUTHOR INFORMATION

Corresponding Author

*E-mail address: josecdscosta@gmail.com.

Funding

We thank the Fundação para a Ciência e a Tecnologia (FCT), Lisbon, Portugal, and the European Social Fund (ESF) for financial support to the CIQ, University of Porto (Projects: PEst-C/QUI/UI0081/2011, FCUP-CIQ-UP-NORTE-07- 0124-FEDER-000065, PTDC/AAC-AMB/121161/2010, UID/QUI/50006/2013). J.C.S.C. also thanks the FCT and the European Social Fund (ESF) under the third Community Support Framework (CSF) for the award of the Research Grant SFRH/BD/74367/2010.

Notes

The authors declare no competing financial interest.

ACKNOWLEDGMENTS

Centro de Materiais da Universidade do Porto (CEMUP) is acknowledged for expert help with the scanning electron microscopy.

REFERENCES

1. Mattox, D. M. *Handbook of Physical Vapor Deposition (PVD) Processing*, 2nd ed.; Elsevier Science: Oxford, 2010.
2. Harsha, K. S. S. *Principles of Physical Vapor Deposition of Thin Films*, 1st ed.; Elsevier: London, 2006.
3. Mahan, J. E. *Physical Vapor Deposition of Thin Films*; Wiley: New York, 2000.
4. Hampden-Smith, M. J.; Kodas, T. T. Chemical Vapor Deposition of Metals: Part 1. An Overview of CVD Processes. *Chem. Vap. Deposition* 1995, *1*, 8−23.
5. Reina, A.; Jia, X.; Ho, J.; Nezich, D.; Son, H.; Bulovic, V.; Dresselhaus, M. S.; Kong, J. Large Area, Few-Layer Graphene Films on Arbitrary Substrates by Chemical Vapor Deposition. *Nano Lett.* 2009, *9*, 30−35.
6. Helmersson, U.; Lattemann, M.; Bohlmark, J.; Ehiasarian, A. P.; Gudmundsson, J. T. Ionized Physical Vapor Deposition (IPVD): A Review of Technology and Applications. *Thin Solid Films* 2006, *513*, 1−24.
7. Li, X.; Magnuson, C. W.; Venugopal, A.; Tromp, R. M.; Hannon, J. B.; Vogel, E. M.; Colombo, L.; Ruoff, R. S. Large-Area Graphene Single Crystals Grown by Low-Pressure Chemical Vapor Deposition of Methane on Copper. *J. Am. Chem. Soc.* 2011, *133*, 2816−2819.
8. Hatalis, M. K.; Greve, D. W. Large Grain Polycrystalline Silicon by Low-Temperature Annealing of Low-Pressure Chemical Vapor Deposited Amorphous Silicon Films. *J. Appl. Phys.* 1988, *63*, 2260−2266.
9. Li, Y.; Mann, D.; Rolandi, M.; Kim, W.; Ural, A.; Hung, S.; Javey, A.; Cao, J.; Wang, D.; Yenilmez, E.; Wang, Q.; Gibbons, J. F.; Nishi, Y.; Dai, H. Preferential Growth of Semiconducting Single-Walled Carbon Nanotubes by a Plasma Enhanced CVD Method. *Nano Lett.* 2004, *4*, 317−321.
10. Hozumi, A.; Takai, O. Preparation of Ultra Water-Repellent Films by Microwave Plasma-Enhanced CVD. *Thin Solid Films* 1997, *303*, 222−225.
11. Lu, J.; Gu, Y.; Grotjohn, T. A.; Schuelke, T.; Asmussen, J. Experimentally Defining the Safe and Efficient, High Pressure Microwave Plasma Assisted CVD Operating Regime for Single Crystal Diamond Synthesis. *Diamond Relat. Mater.* 2013, *37*, 17−28.
12. Wang, C. D.; Yuen, M. F.; Ng, T. W.; Jha, S. K.; Lu, Z. Z.; Kwok, S. Y.; Wong, T. L.; Yang, X.; Lee, C. S.; Lee, S. T.; Zhang, W. J. Plasma-Assisted Growth and Nitrogen Doping of Graphene Films. *Appl. Phys. Lett.* 2012, *100*, 253107.
13. Ozaydin-Ince, G.; Coclite, A. M.; Gleason, K. K. CVD of Polymeric Thin Films: Applications in Sensors, Biotechnology, Microelectronics/Organic Electronics, Microfluidics, MEMS, Composites and Membranes. *Rep. Prog. Phys.* 2012, *75*, 016501.
14. Park, J. S.; Maeng, W.-J.; Kim, H.-S.; Park, J.-S. Review of Recent Developments in Amorphous Oxide Semiconductor Thin-Film Transistor Devices. *Thin Solid Films* 2012, *520*, 1679−1693.
15. Sanders, D. M.; Anders, A. Review of Cathodic Arc Deposition Technology at the Start of the New Millennium. *Surf. Coat. Technol.* 2000, *133−134*, 78−90.
16. Pharr, G. M.; Callahan, D. L.; McAdams, S. D.; Tsui, T. Y.; Anders, S.; Anders, A.; Ager, J. W., III; Brown, I. G.; Bhatia, C. S.; Silva, S. R. P. Robertson, Mechanical Properties and Structure of Very hard Carbon Films Produced by Cathodic-Arc Deposition. *Appl. Phys. Lett.* 1996, *68*, 779−781.
17. Matsumoto, M.; Yamaguchi, N.; Matsubara, H. Low Thermal Conductivity and High

Temperature Stability of ZrO2-Y2O3-La2O3 Coatings Produced by Electron Beam PVD. *Scr. Mater.* 2004, *50*, 867−871.

18. Singh, J.; Wolfe, D. E. Nano and Macro-Structured Component Fabrication by Electron Beam-Physical Vapor Deposition (EB-PVD). *J. Mater. Sci.* 2005, *40*, 1−26.

19. Cantalini, C.; Sun, H. T.; Faccio, M.; Pelino, M.; Santucci, S.; Lozzi, L.; Passacantando, M. NO2 Sensitivity of WO3 Thin Film Obtained by High Vacuum Thermal Evaporation. *Sens. Actuators, B* 1996, *31*, 81−87.

20. Cantalini, C.; Wlodarski, W.; Li, Y.; Passacantando, M.; Santucci, S.; Comini, E.; Faglia, G.; Sberveglieri, G. Investigation on the O3 Sensitivity Properties of WO3 Thin Films Prepared by Sol-Gel, Thermal Evaporation and R.F. Sputtering Techniques. *Sens. Actuators, B* 2000, *64*, 182−188.

21. Singh, R. K.; Narayan, J. Pulsed-Laser Evaporation Technique for Deposition of Thin Films: Physics and Theoretical Model. *Phys. Rev. B: Condens. Matter Mater. Phys.* 1990, *41*, 8843−8859.

22. Dijkkamp, D.; Venkatesan, T.; Wu, X. D.; Shaheen, S. A.; Jisrawi, N.; Min-Lee, Y. H.; McLean, W. L.; Croft, M. Preparation of Y- Ba-Cu Oxide Superconductor Thin Films Using Pulsed Laser Evaporation From High T C Bulk Material. *Appl. Phys. Lett.* 1987, *51*, 619−621.

23. Sato, H.; Minami, T.; Takata, S.; Yamada, T. Transparent Conducting P-Type NiO Thin Films Prepared by Magnetron Sputtering. *Thin Solid Films* 1993, *236*, 27−31.

24. Kitano, M.; Funatsu, K.; Matsuoka, M.; Ueshima, M.; Anpo, M. Preparation of Nitrogen-Substituted TiO2 Thin Films Photocatalysts by the Radio Frequency Magnetron Sputtering Deposition Method and their Photocatalytic Reactivity Under Visible Light Irradiation. *J. Phys. Chem. B* 2006, *110*, 25266−25272.

25. Costa, J. C. S.; Santos, L. M. N. B. F. Hole Transport Materials Based Thin Films: Topographic Structures and Phase Transition Thermodynamics of Triphenylamine Derivatives. *J. Phys. Chem. C* 2013, *117*, 10919−10928.

26. Costa, J. C. S.; Lima, C. F. R. A. C.; Santos, L. M. N. B. F. Electron Transport Materials for Organic Light-Emitting Diodes: Understanding the Crystal and Molecular Stability of the Tris(8-hydroxyquinolines) of Al, Ga, and. *J. Phys. Chem. C* 2014, *118*, 21762− 21769.

27. Selvakumar, N.; Barshilia, H. C. Review of Physical Vapor Deposited (PVD) Spectrally Selective Coatings for Mid- and High- Temperature Solar Thermal Applications. *Sol. Energy Mater. Sol. Cells* 2012, *98*, 1−23.

28. Dimitrakopoulos, C. D.; Malenfant, P. R. L. Organic Thin Film Transistors for Large Area Electronics. *Adv. Mater.* 2002, *14*, 99−117.

29. Gu, G.; Burrows, P. E.; Venkatesh, S.; Forrest, S. R.; Thompson, M. E. Vacuum-Deposited, Nonpolymeric Flexible Organic Light- Emitting Devices. *Opt. Lett.* 1997, *22*, 172−174.

30. Kelley, T. W.; Baude, P. F.; Gerlach, C.; Ender, D. E.; Muyres, D.; Haase, M. A.; Vogel, D. E.; Theiss, S. D. Recent Progress in Organic Electronics: Materials, Devices, and Processes. *Chem. Mater.* 2004, *16*, 4413−4422.

31. Santos, L. M. N. B. F.; Lima, L. M. S. S.; Lima, C. F. R. A. C.; Magalhães, F. D.; Torres, M. C.; Schröder, B.; Ribeiro da Silva, M. A. V. New Knudsen Effusion Apparatus with Simultaneous Gravimetric and Quartz Crystal Microbalance Mass Loss Detection. *J. Chem. Thermodyn.* 2011, *43*, 834−843.

32. Ribeiro da Silva, M. A. V.; Monte, M. J. S. The Construction, Testing and Use of a New Knudsen Effusion Apparatus. *Thermochim. Acta* 1990, *171*, 169−183.

33. Ribeiro da Silva, M. A. V.; Monte, M. J. S.; Santos, L. M. N. B. F. The Design, Construction, and Testing of a New Knudsen Effusion Apparatus. *J. Chem. Thermodyn.* 2006, *38*, 778−787.

34. Clausing, P. Über Die Strömung Sehr Verdünnter Gase Durch Röhren Von Beliebiger Länge. *Ann. Phys.* 1932, *404*, 961−989.

35. Dushman, S. *Scientific Foundations of Vacuum Technique* 2, 2nd ed.; J. Willey; A. Inc: New York, 1962.

36. DeMarcus, W. C.; Hopper, E. H. Knudsen Flow Through a Circular Capillary. *J. Chem. Phys.* 1955, *23*, 1344−1344.

37. Monte, M. J. S.; Santos, L. M. N. B. F.; Fulem, M.; Fonseca, J. M. S.; Sousa, C. A. D. New Static Apparatus and Vapor Pressure of Reference Materials: Naphthalene, Benzoic Acid, Benzophenone, and Ferrocene. *J. Chem. Eng. Data* 2006, *51*, 757−766.

38. de Kruif, C. G. Enthalpies of Sublimation and Vapor Pressures of 11 Polycyclic Hydrocarbons. *J. Chem. Thermodyn.* 1980, *12*, 243− 248.

39. Lima, L. M. S. S.; Santos, L. M. N. B. F.; Ribeiro da Silva, M. A. V. *Estudo Energético de Alguns Hidrocarbonetos Aromáticos Policíclicos e Polifenilos.* Ph.D. Thesis, Faculdade de Ciências, Universidade do Porto, 2009.

40. Roux, M. V.; Temprado, M.; Chickos, J. S.; Nagano, Y. Critically Evaluated Thermochemical Properties of Polycyclic Aromatic Hydrocarbons. *J. Phys. Chem. Ref. Data* 2008, *37*, 1855−1996.

41. Kyiobayashi, T.; Minas da Piedade, M. E. The Standard Molar Enthalpy of Sublimation of 5-Bis-Pentamethylcyclopentadienyl Iron Measured With an Electrically Calibrated Vacuum-Drop Sublimation Microcalorimetric Apparatus. *J. Chem. Thermodyn.* 2001, *33*, 11−21.

42. Sabbah, R.; Xu-wu, A.; Chickos, J. S.; Leitao, M. L. P.; Roux, M. V.; Torres, L. A. Reference Materials for Calorimetry and Differential Thermal Analysis. *Thermochim. Acta* 1999, *331*, 93−204.

43. Zielenkiewicz, W.; Perlovich, G. L.; Wszelaka-Rylik, M. The Vapor Pressure and the Enthalpy of Sublimation: Determination by Inert Gas Flow Method. *J. Therm. Anal. Calorim.* 1999, *57*, 225−234.

44. de Kruif, C. G.; Blok, J. G. The Vapor Pressure of Benzoic Acid. *J. Chem. Thermodyn.* 1982, *14*, 201−206.

45. Oja, V.; Suuberg, E. M. Development of a Nonisothermal Knudsen Effusion Method and Application to PAH and Cellulose Tar Vapor Pressure Measurement. *Anal. Chem.* 1997, *69*, 4619−4626.

46. Rordorf, B. F. Thermodynamic and Thermal Properties of Polychlorinated Compounds: The Vapor Pressures and Flow Tube Kinetics of Ten Dibenzo-Para-Dioxines. *Chemosphere* 1985, *14*, 885−892.

47. Hoyer, H.; Peperle, W. *Z. Elektrochem.* 1958, *62*, 61−66.

48. Ribeiro da Silva, M. A. V.; Ferrão, M. L. C. C. H.; Monte, M. J. S.; Gonçalves, J. M.; Jiye, F. Standard Molar Enthalpy of Formation, Vapor Pressures, and Standard Molar Enthalpy of Sublimation of Benzanthrone. *J. Chem. Thermodyn.* 1999, *31*, 1067−1075.

49. Burkinshaw, P. M.; Mortimer, C. T. Enthalpies of Sublimation of Transition Metal Complexes. *J. Chem. Soc., Dalton Trans.* 1984, 75− 77.

50. Verevkin, S. P. Thermochemistry of Substituted Benzenes. Experimental Standard Molar Enthalpies of Formation of *o*-, *m*-, *p*- Terphenyls, and 1,3,5-Triphenylbenzene. *J. Chem. Thermodyn.* 1997, *29*, 1495−1501.

51. Malaspina, L.; Bardi, G.; Gigli, R. Simultaneous Determination by Knudsen-Effusion Microcalorimetric Technique of the Vapor Pressure and Enthalpy of Vaporization of Pyrene and 1,3,5-Triphenylbenzene. *J. Chem. Thermodyn.* 1974, *6*, 1053−1064.

52. Wakayama, N.; Inokuchi, H. Heats of Sublimation of Polycyclic Aromatic Hydrocarbons and Their Molecular Packings. *Bull. Chem. Soc. Jpn.* 1967, *40*, 2267−2271.

53. Goldfarb, J. L.; Suuberg, E. M. Vapor Pressures and Enthalpies of Sublimation of Ten Polycyclic Aromatic Hydrocarbons Determined via the Knudsen Effusion Method. *J. Chem. Eng. Data* 2008, *53*, 670−676.

54. Oja, V.; Suuberg, E. M. Vapor Pressures and Enthalpies of Sublimation of Polycyclic Aromatic Hydrocarbons and Their Derivatives. *J. Chem. Eng. Data* 1998, *43*, 486−492.

55. Inokuchi, I.; Shiba, S.; Handa, T.; Akamatu, H. Heats of Sublimation of Condensed Polynuclear Aromatic Hydrocarbons. *Bull. Chem. Soc. Jpn.* 1952, *25*, 299−302.

56. Floro, J. A.; Hearne, S. J.; Hunter, J. A.; Kotula, P.; Chason, E.; Seel, S. C.; Thompson, C. V. The Dynamic Competition Between Stress Generation and Relaxation Mechanisms During Coalescence of Volmer-Weber Thin Films. *J. Appl. Phys.* 2001, *89*, 4886−4897.

57. Bauer, E.; van der Merwe, J. Structure and Growth of Crystalline Superlattices: From Monolayer to Superlattice. *Phys. Rev. B: Condens. Matter Mater. Phys.* 1986, *33*, 3657−3671.

58. Martin, P. M. *Handbook of Deposition Technologies for Films and Coatings: Science Applications and Technology*, 3rd ed.; Elsevier Science: New York, 2009.

59. Nix, W. D.; Clemens, B. M. Crystallite Coalescence: a Mechanism for Intrinsic Tensile Stresses in Thin Films. *J. Mater. Res.* 1999, *14*, 3467−3473.

60. Tello, J. S.; Bower, A. F.; Chason, E.; Sheldon, B. W. Kinetic Model of Stress Evolution during Coalescence and Growth of Polycrystalline Thin Films. *Phys. Rev. Lett.* 2007, *98*, 216104.

61. Fletcher, N. H. Size Effect in Heterogeneous Nucleation. *J. Chem. Phys.* 1958, *29*, 572−576.

62. Turnbull, D. Kinetics of Heterogeneous Nucleation. *J. Chem. Phys.* 1950, *18*, 198−203.

63. Lima, C. F. R. A. C.; Costa, J. C. S.; Melo, A.; Tavares, H. R.; Silva, A. M. S.; Santos, L. M. N. B. F. Effect of Self-Association on the Phase Stability of Triphenylamine Derivatives. *J. Phys. Chem. A* 2015, *119*, 6676−6682.

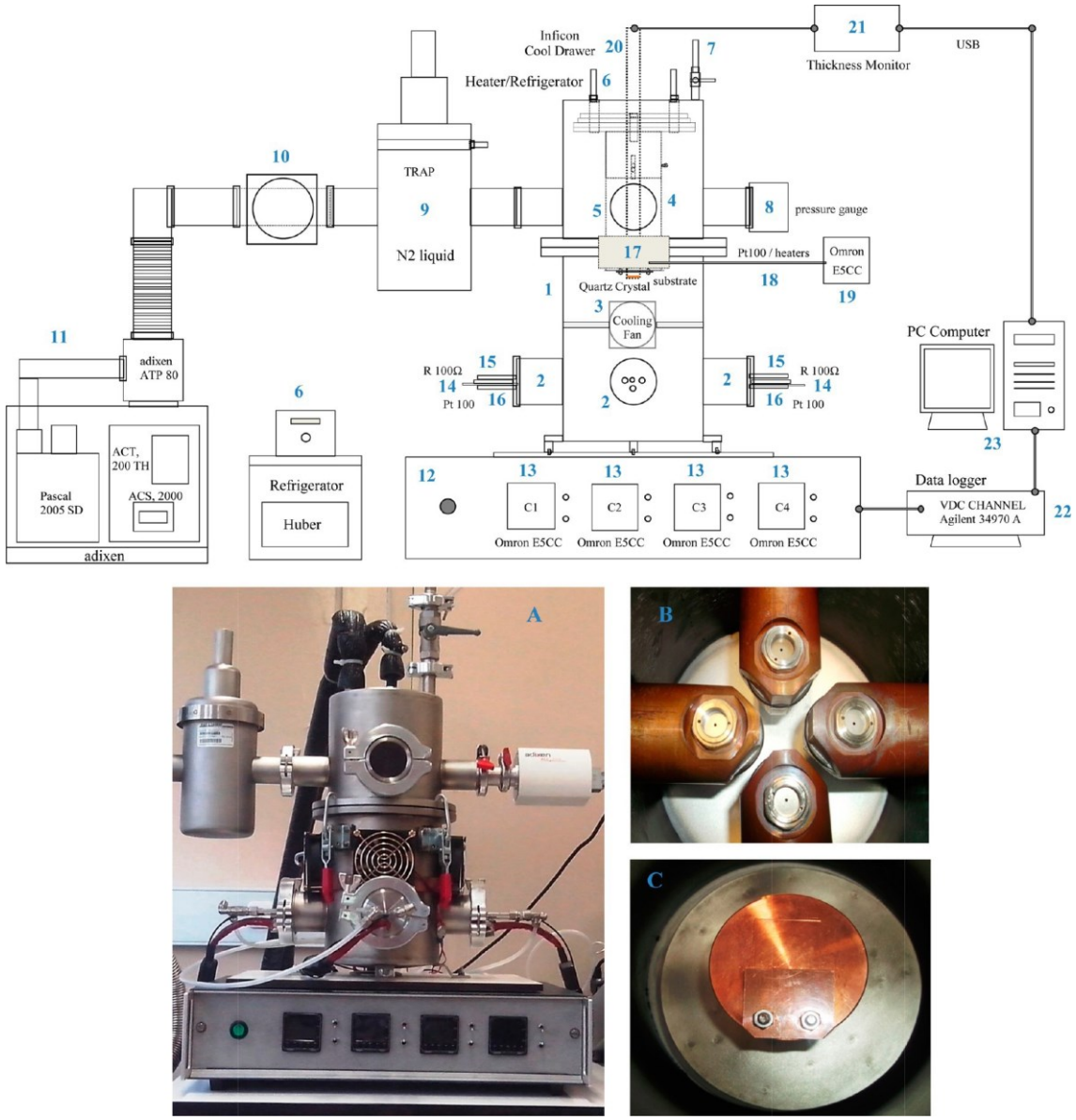

Figure 1. Schematic representation and images of ThinFilmVD system: 1, vacuum chamber; 2, ovens; 3, cooling fans; 4, sapphire window; 5, substrates support system (refrigerated copper tube); 6, substrates cooling system; 7, gas inlet valve; 8, pressure gauge; 9, N_2 (l) metallic trap; 10, vacuum valve; 11, turbomolecular pump; 12, instrumentation box; 13, temperature controllers (ovens); 14, Pt100 sensors; 15, heaters; 16, air cooling system; 17, stainless steel disk; 18, Pt100 sensor and heaters; 19, temperature controller (substrate); 20, cooled quartz crystal microbalance; 21, thickness monitor; 22, data acquisition system; 23, personal computer; A, image of the vacuum chamber; B, image of the four ovens with the Knudsen cells; C, image of the refrigerated copper tube.

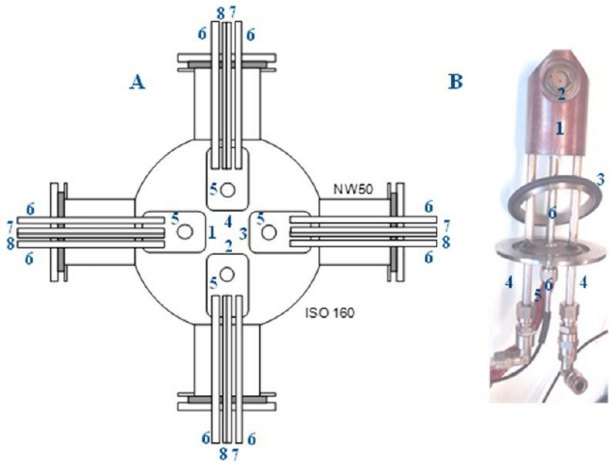

Figure 2. A, schematic representation of the ovens: 1, 2, 3, 4, individual ovens; 5, cavity of the Knudsen cell screwing; 6, air cooling tube; 7, heater; 8, Pt100 sensor; B, Image of an individual oven (top view): 1, copper block; 2, Knudsen cell; 3, Viton O-ring; 4, cooling system; 5, heater; 6, Pt100.

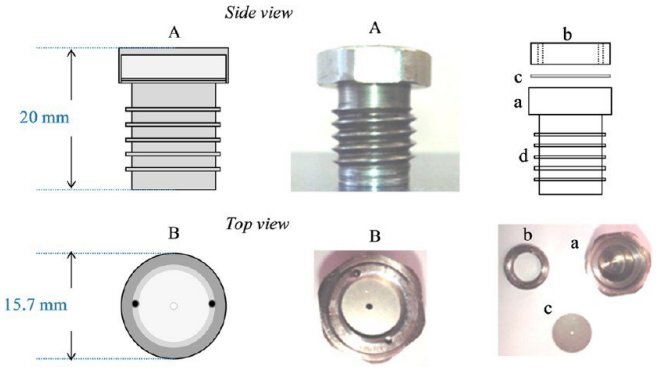

Figure 3. Images and schematic representation of a Knudsen effusion cell used in ThinFilmVD: A, side view; B, top view; a, the cell body; b, the cell lid; c, the disk with an orifice; d, screwing system.

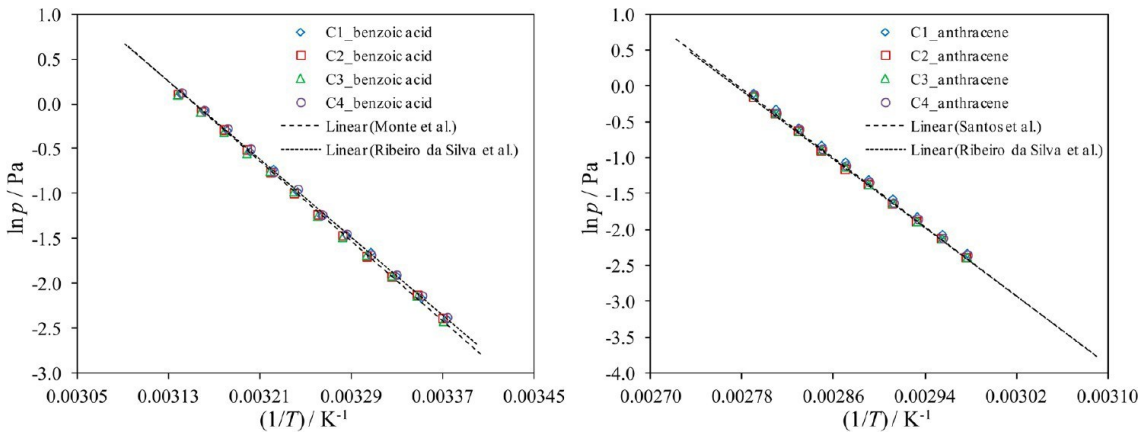

Figure 4. Plots of ln p against $1/T$ for benzoic acid and anthracene. Plots obtained by Monte, Santos, and Ribeiro da Silva et al. are presented for comparison.[31,33,37]

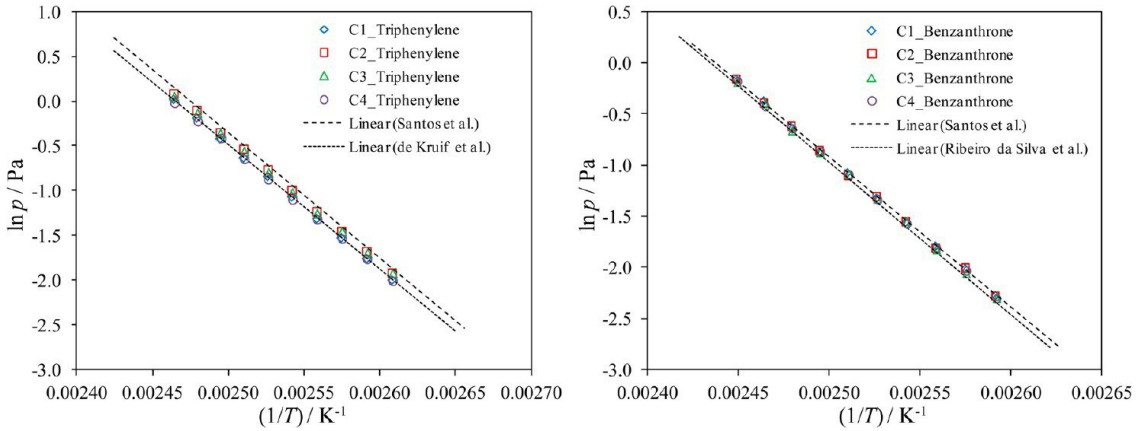

Figure 5. Plots of ln p against $1/T$ for triphenylene and benzanthrone. Plots obtained by de Kruif, Santos and Ribeiro da Silva et al. are presented for comparison.[31,37,38]

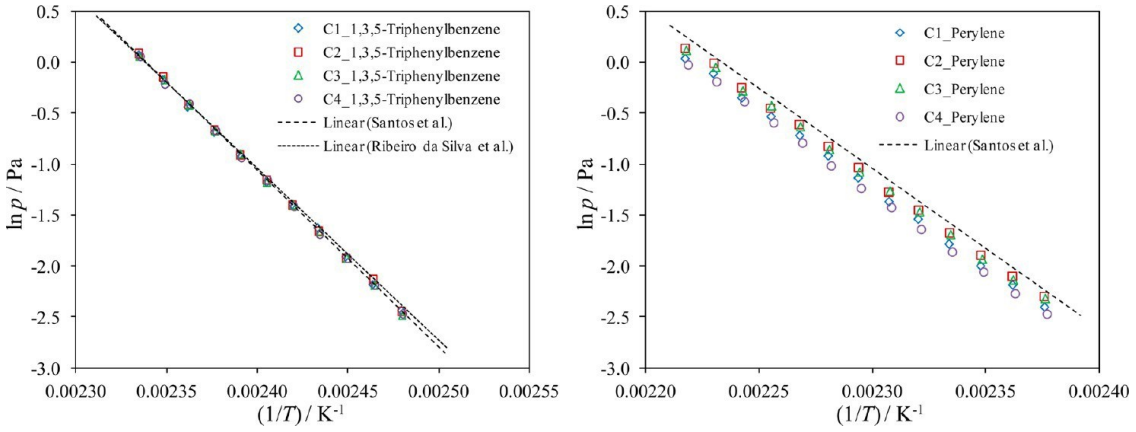

Figure 6. Plots of ln p against $1/T$ for 1,3,5-triphenylbenzene and perylene. Plots obtained by Santos and Ribeiro da Silva et al. are presented for comparison.[31,33,39]

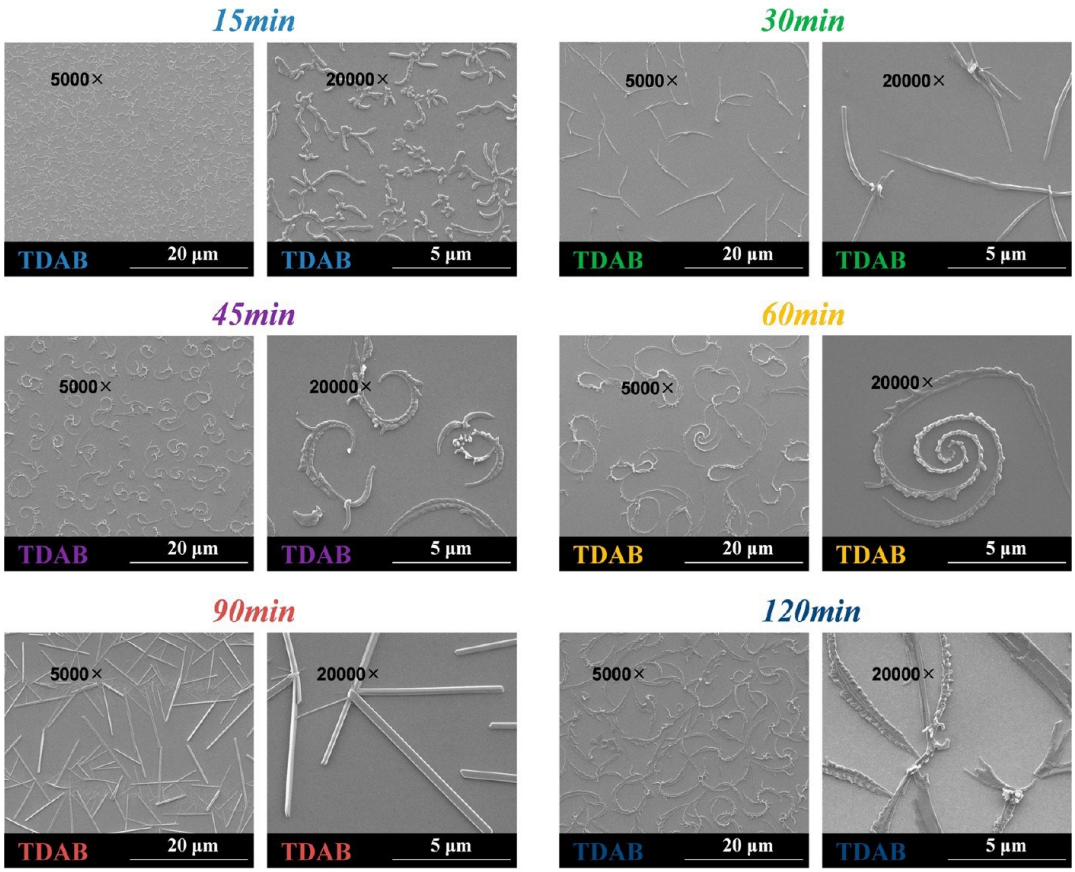

Figure 7. Topographic images obtained by SEM of the nanostructures of TDAB deposited by vacuum deposition (C1, $p \approx 0.5$ Pa, $t \approx 15/30/45/60/90/120$ min, $h \approx 25$ cm, T(substrate) ≈ 298 K).

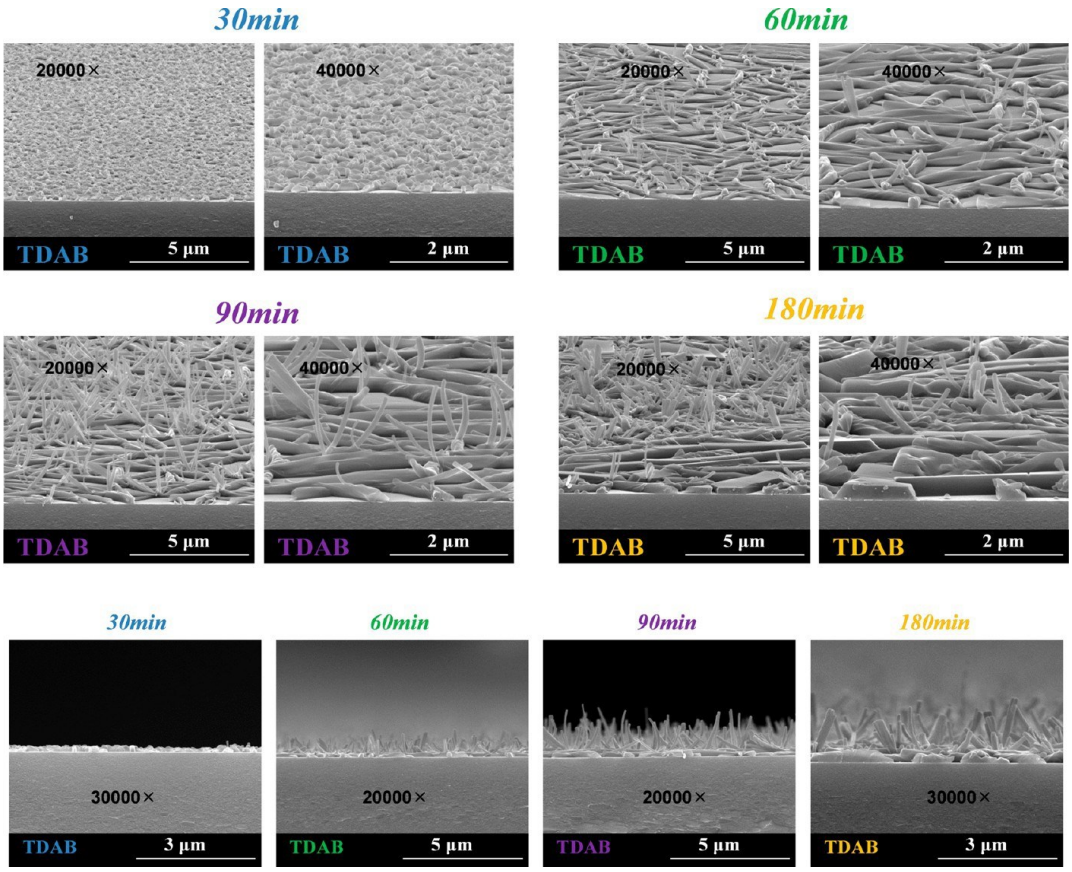

Figure 8. Topographic images obtained by SEM of the nanostructures of TDAB deposited by vacuum deposition (C2 and C4, $p \approx 0.5$ Pa, $t \approx 30/\ 60/90/180$ min, $h \approx 10$ cm, T(substrate) ≈ 298 K). The images given at the bottom are referred to the cross-sectional SEM images of the substrate with the nanostructures deposited.

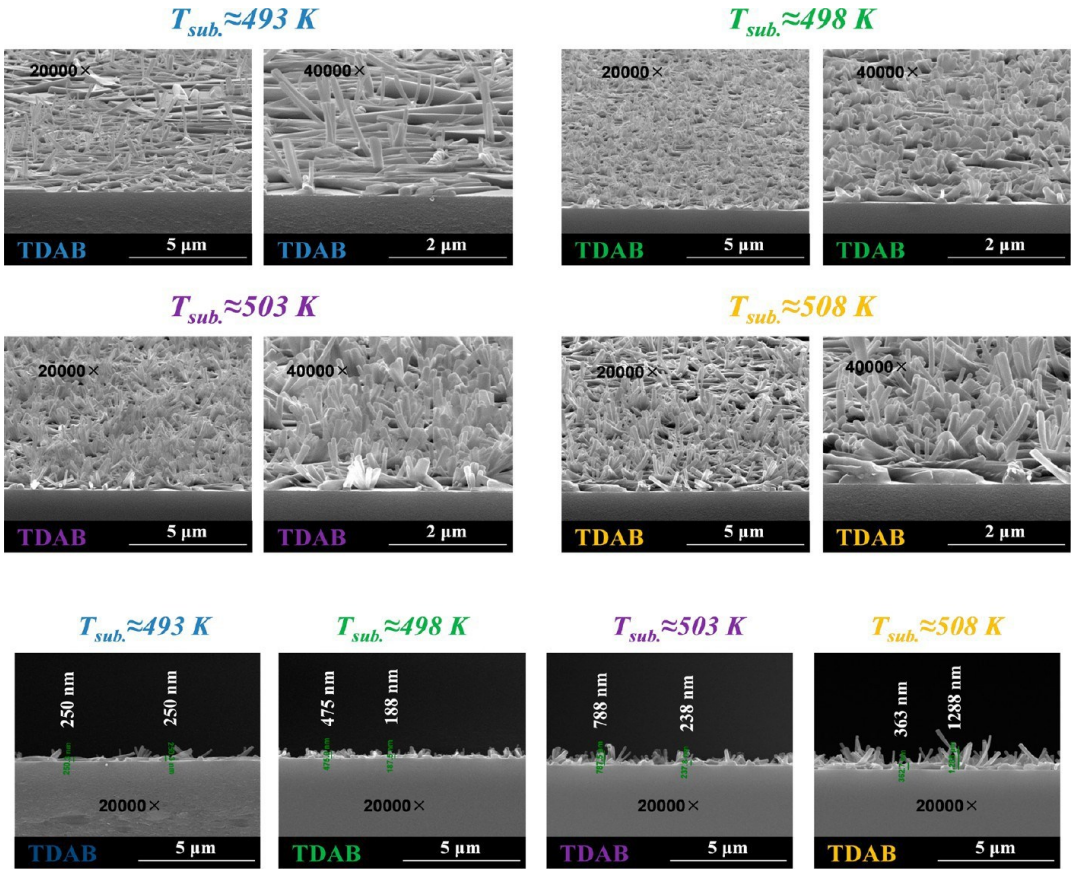

Figure 9. Topographic images obtained by SEM of the nanostructures of TDAB deposited by vacuum deposition (C2 and C4, T(sub) ≈ 493/498/ 503/508 K, t ≈ 60 min, h ≈ 10 cm, T(substrate) ≈ 298 K). The images given at the bottom are referred to the cross-sectional SEM images of the substrate with the nanostructures deposited

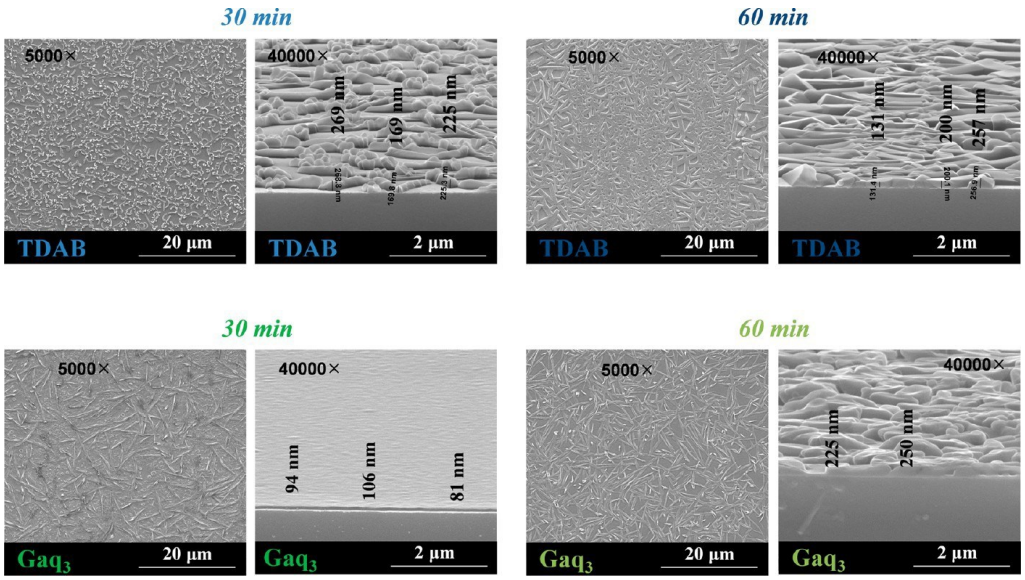

Figure 10. Topographic images obtained by SEM of the nanostructures/thin films of TDAB and *mer*-Gaq3 deposited by vacuum deposition (C2 and C4, $p \approx 0.5$ Pa, $t \approx 30/60$ min, $h \approx 10$ cm, T(substrate) ≈ 283 K).

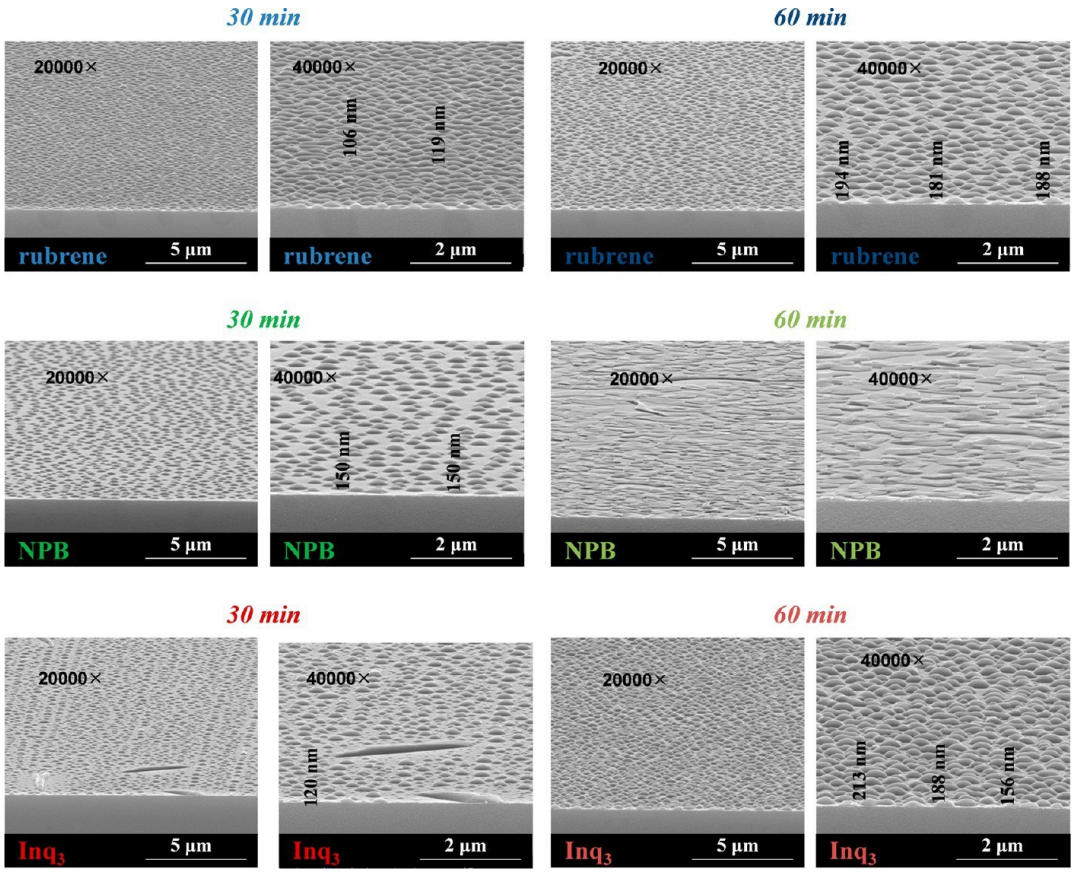

Figure 11. Topographic images obtained by SEM of the nanostructures/thin films of rubrene, NPB, and *fac*-Inq3 deposited by vacuum deposition (C2, $p \approx 0.5$ Pa, $t \approx 30/60$ min, $h \approx 10$ cm, T(substrate) ≈ 283 K).

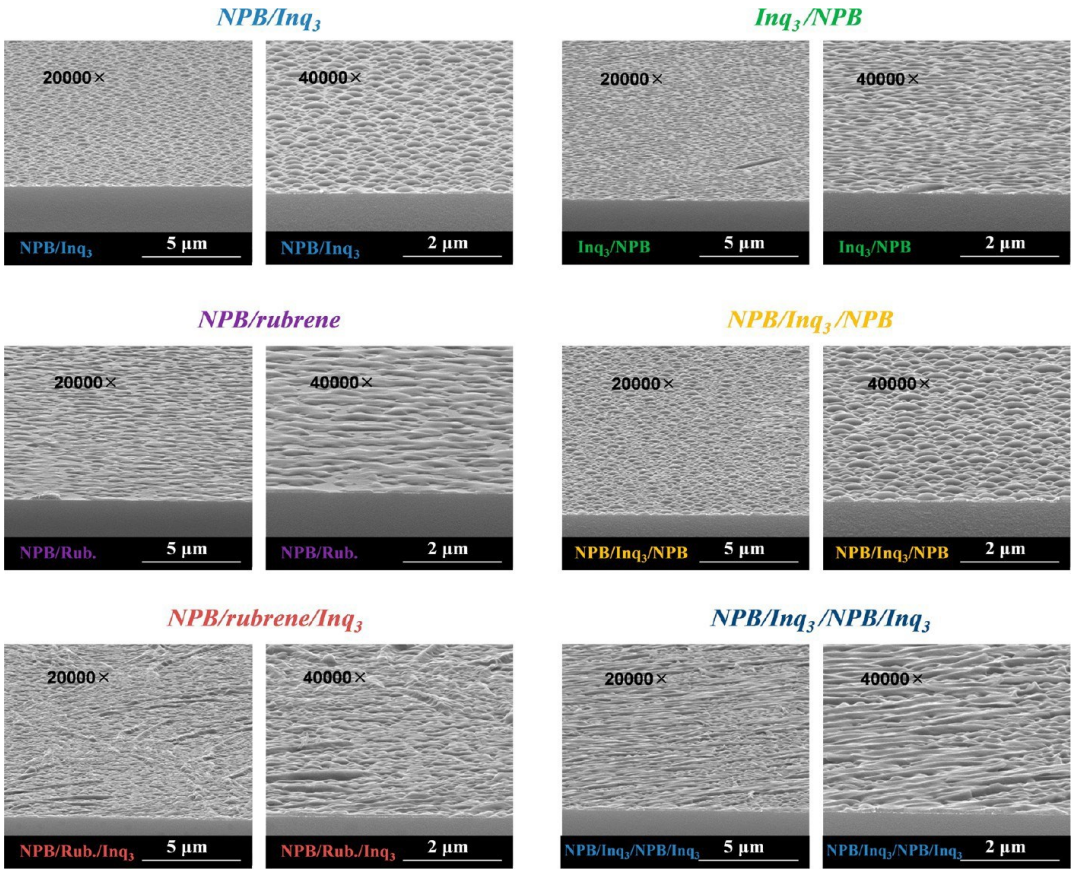

Figure 12. Topographic images obtained by SEM of the composite thin films of rubrene, NPB, and *fac*-Inq3 deposited by vacuum deposition (C2, *p*

≈ 0.5 Pa, *t* ≈ 30/60 min, *h* ≈ 10 cm, *T*(substrate) ≈ 283 K).

Table 1. Experimental Data of Vapor Pressures for Benzoic Acid

T/K	p/Pa	T/K	p/Pa	T/K	p/Pa	T/K	p/Pa
Knudsen Cell C1		Knudsen Cell C2		Knudsen Cell C3		Knudsen Cell C4	
296.41	0.0908	296.71	0.0919	296.67	0.0889	296.36	0.0928
298.39	0.115	298.69	0.119	298.71	0.118	298.31	0.118
300.38	0.148	300.70	0.146	300.69	0.148	300.31	0.149
302.39	0.192	302.69	0.183	302.73	0.186	302.33	0.186
304.37	0.233	304.64	0.231	304.67	0.227	304.30	0.235
306.36	0.287	306.67	0.292	306.72	0.287	306.30	0.291
308.37	0.377	308.64	0.369	308.68	0.378	308.30	0.387
310.37	0.484	310.61	0.467	310.67	0.474	310.31	0.469
312.35	0.588	312.61	0.602	312.64	0.579	312.29	0.608
314.34	0.746	314.58	0.751	314.61	0.733	314.27	0.761
316.36	0.935	316.58	0.920	316.66	0.918	316.29	0.933
318.36	1.116	318.61	1.114	318.68	1.111	318.29	1.136

Table 2. Experimental Data of Vapor Pressures for Anthracene

T/K	p/Pa	T/K	p/Pa	T/K	p/Pa	T/K	p/Pa
Knudsen Cell C1		Knudsen Cell C2		Knudsen Cell C3		Knudsen Cell C4	
335.95	0.0976	336.03	0.0920	335.96	0.0925	335.87	0.0951
338.42	0.127	338.51	0.120	338.43	0.120	338.33	0.120
340.97	0.162	341.03	0.152	340.96	0.152	340.86	0.157
343.47	0.208	343.52	0.194	343.45	0.197	343.35	0.196
345.98	0.272	346.01	0.255	345.96	0.255	345.86	0.262
348.42	0.348	348.46	0.315	348.43	0.326	348.30	0.330
350.99	0.439	351.01	0.406	350.94	0.412	350.87	0.416
353.47	0.560	353.48	0.537	353.42	0.533	353.36	0.549
355.98	0.727	356.01	0.684	355.95	0.687	355.86	0.687
358.47	0.908	358.48	0.862	358.44	0.894	358.36	0.887

Table 3. Experimental Data of Vapor Pressures for Triphenylene

T/K	p/Pa	T/K	p/Pa	T/K	p/Pa	T/K	p/Pa
Knudsen Cell C1		Knudsen Cell C2		Knudsen Cell C3		Knudsen Cell C4	
383.47	0.136	383.45	0.147	383.37	0.146	383.36	0.134
385.95	0.173	385.93	0.187	385.85	0.183	385.87	0.171
388.47	0.218	388.41	0.234	388.35	0.234	388.34	0.215
390.92	0.270	390.91	0.292	390.86	0.285	390.84	0.267
393.47	0.345	393.43	0.370	393.37	0.360	393.34	0.332
395.95	0.433	395.90	0.466	395.83	0.451	395.84	0.417
398.46	0.533	398.42	0.586	398.35	0.572	398.33	0.523
400.94	0.659	400.88	0.704	400.86	0.699	400.75	0.662
403.44	0.832	403.39	0.903	403.32	0.876	403.26	0.798
405.93	1.03	405.88	1.09	405.83	1.06	405.77	0.979

Table 4. Experimental Data of Vapor Pressures for Benzanthrone

T/K	p/Pa	T/K	p/Pa	T/K	p/Pa	T/K	p/Pa
Knudsen Cell C1		Knudsen Cell C2		Knudsen Cell C3		Knudsen Cell C4	
385.97	0.103	385.95	0.103	385.85	0.100	385.84	0.0999
388.47	0.134	388.43	0.135	388.35	0.128	388.31	0.131
390.95	0.167	390.92	0.164	390.84	0.162	390.82	0.164
393.47	0.211	393.45	0.212	393.35	0.212	393.33	0.208
395.98	0.266	395.95	0.271	395.87	0.265	395.82	0.263
398.49	0.342	398.43	0.333	398.35	0.337	398.31	0.335
400.98	0.419	400.94	0.425	400.88	0.417	400.81	0.419
403.50	0.536	403.45	0.540	403.36	0.516	403.32	0.525
405.94	0.691	405.92	0.677	405.83	0.674	405.76	0.654
408.47	0.853	408.44	0.855	408.34	0.828	408.28	0.837

Table 5. Experimental Data of Vapor Pressures for 1,3,5-Triphenylbenzene

T/K	p/Pa	T/K	p/Pa	T/K	p/Pa	T/K	p/Pa
Knudsen Cell C1		Knudsen Cell C2		Knudsen Cell C3		Knudsen Cell C4	
403.42	0.0881	403.41	0.0873	403.33	0.0840	403.26	0.0852
406.02	0.114	405.95	0.120	405.84	0.113	405.81	0.113
408.48	0.149	408.43	0.147	408.36	0.147	408.29	0.147
411.08	0.198	410.98	0.192	410.84	0.191	410.86	0.186
413.45	0.249	413.44	0.248	413.35	0.249	413.27	0.244
415.90	0.310	415.89	0.317	415.87	0.310	415.74	0.315
418.46	0.407	418.43	0.405	418.35	0.409	418.28	0.394
420.95	0.506	420.92	0.517	420.83	0.512	420.75	0.513
423.57	0.648	423.48	0.663	423.36	0.660	423.34	0.668
426.01	0.844	425.97	0.871	425.84	0.847	425.79	0.811
428.43	1.08	428.44	1.10	428.37	1.07	428.25	1.06

Table 6. Experimental Data of Vapor Pressures for Perylene

T/K	p/Pa	T/K	p/Pa	T/K	p/Pa	T/K	p/Pa
Knudsen Cell C1		Knudsen Cell C2		Knudsen Cell C3		Knudsen Cell C4	
420.89	0.0910	420.92	0.101	420.83	0.0990	420.69	0.0850
423.40	0.113	423.43	0.123	423.35	0.119	423.19	0.104
425.95	0.137	425.94	0.151	425.81	0.146	425.70	0.128
428.49	0.169	428.45	0.188	428.35	0.185	428.22	0.156
431.01	0.216	430.98	0.236	430.88	0.232	430.74	0.195
433.41	0.256	433.43	0.281	433.32	0.284	433.19	0.242
435.98	0.323	435.95	0.358	435.84	0.342	435.71	0.292
438.50	0.401	438.49	0.441	438.39	0.427	438.24	0.363
440.94	0.490	440.98	0.545	440.87	0.535	440.69	0.455
443.40	0.590	443.46	0.640	443.36	0.655	443.17	0.555
445.96	0.708	445.97	0.783	445.86	0.758	445.71	0.681
448.47	0.900	448.41	0.995	448.25	0.955	448.17	0.830
450.98	1.04	450.98	1.15	450.87	1.13	450.69	0.978

Table 7. Sublimation Results for the Compounds Studied[a]

Knudsen cell	a	b / K	r^2	$\langle T \rangle$ / K	$p(\langle T \rangle)$ / Pa	$\Delta_s^g H_m^o(\langle T \rangle)$ / kJ·mol^{-1}	$\Delta_s^g S_m(\langle T \rangle; p(T))$ / J·K^{-1}·mol^{-1}
			Benzoic Acid				
C1	34.34 ± 0.26	10890 ± 79	0.9994	307.37	0.336	90.5 ± 0.7	294.4 ± 2.6
C2	34.37 ± 0.28	10911 ± 86	0.9994	307.64	0.334	90.7 ± 0.7	294.8 ± 2.8
C3	34.24 ± 0.26	10873 ± 81	0.9994	307.68	0.332	90.4 ± 0.7	293.8 ± 2.7
C4	34.35 ± 0.26	10889 ± 79	0.9995	307.31	0.339	90.5 ± 0.7	294.5 ± 2.6
			Anthracene				
C1	33.23 ± 0.17	11947 ± 58	0.9998	347.21	0.308	99.3 ± 0.5	286.0 ± 2.0
C2	33.35 ± 0.30	12012 ± 105	0.9994	347.25	0.289	99.9 ± 0.9	287.7 ± 2.7
C3	33.57 ± 0.27	12083 ± 95	0.9995	347.19	0.292	100.5 ± 0.8	289.5 ± 2.6
C4	33.28 ± 0.28	11977 ± 97	0.9995	347.10	0.293	99.6 ± 0.8	286.9 ± 2.6
			Triphenylene				
C1	34.44 ± 0.13	13970 ± 49	0.9999	394.70	0.385	116.2 ± 0.4	294.4 ± 1.6
C2	34.47 ± 0.20	13953 ± 77	0.9998	394.66	0.413	116.0 ± 0.6	293.9 ± 2.0
C3	34.09 ± 0.21	13809 ± 81	0.9997	394.60	0.405	114.8 ± 0.7	290.9 ± 2.1
C4	34.12 ± 0.21	13850 ± 82	0.9997	394.57	0.375	115.2 ± 0.7	292.0 ± 2.1
			Benzanthrone				
C1	35.99 ± 0.29	14768 ± 115	0.9995	397.22	0.305	122.8 ± 1.0	309.1 ± 2.5
C2	35.97 ± 0.28	14761 ± 109	0.9996	397.19	0.303	122.7 ± 0.9	308.9 ± 2.4
C3	36.01 ± 0.25	14783 ± 100	0.9996	397.10	0.296	122.9 ± 0.8	309.5 ± 2.3
C4	35.95 ± 0.18	14757 ± 71	0.9998	397.06	0.297	122.7 ± 0.6	309.0 ± 1.9
			1,3,5-Triphenylbenzene				
C1	40.16 ± 0.28	17184 ± 115	0.9996	415.98	0.317	142.9 ± 1.0	343.5 ± 2.4
C2	40.50 ± 0.29	17320 ± 122	0.9996	415.94	0.320	144.0 ± 1.0	346.2 ± 2.4
C3	40.73 ± 0.21	17418 ± 89	0.9998	415.85	0.315	144.8 ± 0.7	348.2 ± 2.1
C4	40.49 ± 0.24	17318 ± 100	0.9997	415.79	0.313	144.0 ± 0.8	346.3 ± 2.2
			Perylene				
C1	34.64 ± 0.23	15595 ± 102	0.9995	435.95	0.322	129.7 ± 0.8	297.5 ± 2.1
C2	34.74 ± 0.24	15595 ± 106	0.9995	435.95	0.355	129.7 ± 0.9	297.5 ± 2.2
C3	34.82 ± 0.25	15637 ± 110	0.9995	435.84	0.348	130.0 ± 0.9	298.3 ± 2.2
C4	34.82 ± 0.22	15695 ± 98	0.9996	435.70	0.299	130.5 ± 0.8	299.5 ± 2.1

[a]The uncertainties of the parameters a and b were obtained by the least-squares method from the fitting. The uncertainties of the thermodynamic parameters were calculated by using the rules of propagation of uncertainty. a and b are from the Clausius–Clapeyron equation, $\ln(p/\mathrm{Pa}) = a - b \cdot (\mathrm{K}/T)$, and $b = \Delta_s^g H_m^o(\langle T \rangle)/R$; $R = 8.3144621$ J·K^{-1}·mol^{-1}.

Table 8. Values of the Standard Molar Enthalpies, $\Delta_s^g H_m^o$, Entropies, $\Delta_s^g S_m^o$, and Gibbs Energies, $\Delta_s^g G_m^o$, of Sublimation, at T = 298.15 K, for the Compounds Studied Together with Some Selected Literature Data[a]

ThinFilmVD/literature data	$\Delta_s^g H_m^o$ kJ·mol^{-1}	$\Delta_s^g S_m^o$ J·K^{-1}·mol^{-1}	$\Delta_s^g G_m^o$ kJ·mol^{-1}	ThinFilmVD/literature data	$\Delta_s^g H_m^o$ kJ·mol^{-1}	$\Delta_s^g S_m^o$ J·K^{-1}·mol^{-1}	$\Delta_s^g G_m^o$ kJ·mol^{-1}
	Benzoic Acid				Anthracene		
Test_C1	90.9 ± 0.7	191.0 ± 2.7	34.0 ± 1.0	Test_C1	100.6 ± 0.7	184.6 ± 2.5	45.6 ± 1.0
Test_C2	91.1 ± 0.7	191.3 ± 2.8	34.1 ± 1.1	Test_C2	101.2 ± 1.0	185.8 ± 3.1	45.8 ± 1.4
Test_C3	90.8 ± 0.7	190.3 ± 2.7	34.1 ± 1.0	Test_C3	101.8 ± 0.9	187.7 ± 3.0	45.9 ± 1.3
Test_C4	90.9 ± 0.7	191.1 ± 2.7	33.9 ± 1.0	Test_C4	100.9 ± 0.9	185.1 ± 3.0	45.7 ± 1.3
ThinFilmVD (average)	**90.9 ± 0.7**	**190.9 ± 2.7**	**34.0 ± 1.1**	**ThinFilmVD** (average)	**101.1 ± 0.9**	**185.8 ± 2.9**	**45.8 ± 1.2**
Ribeiro da Silva et al.[33]	90.4 ± 0.5	189 ± 2	34.0 ± 0.8	Ribeiro da Silva et al.[33]	100.2 ± 0.4	183.0 ± 1.0	45.6 ± 0.3
Monte et al.[37]	91.5 ± 0.5	192.5 ± 2.3	34.0 ± 0.9	Santos et al.[31]	100.6 ± 0.9	183.8 ± 2.6	45.8 ± 1.2
Ribeiro da Silva et al.[32]	89.2 ± 0.8	185.5 ± 2.7	33.9 ± 1.1	Oja/Suuberg[45]	100.7	183.4	46.0
Kyiobayashi et al.[41]	88.3 ± 0.5			Oja/Suuberg[45]	101.8	187.0	46.0
Sabbah et al.[42]	89.7 ± 1.0			de Kruif[38]	102.0 ± 1.0	187.4 ± 2.8	46.1 ± 1.3
Zielenkiewicz et al.[43]	92.0 ± 0.5			de Kruif[38]	101.3 ± 1.0	185.5 ± 2.8	46.0 ± 1.3
de Kruif[44]	92.0 ± 0.2			Rordorf[46]	100.0	182.3	45.6
	Triphenylene				Benzanthrone		
Test_C1	120.1 ± 0.5	201.9 ± 1.7	59.8 ± 0.7	Test_C1	125.7 ± 1.3	211.8 ± 3.6	62.5 ± 1.7
Test_C2	119.9 ± 0.7	202.0 ± 2.1	59.6 ± 0.9	Test_C2	125.6 ± 1.3	211.6 ± 3.5	62.5 ± 1.7
Test_C3	118.6 ± 0.7	198.8 ± 2.2	59.4 ± 1.0	Test_C3	125.8 ± 1.2	212.0 ± 3.4	62.6 ± 1.6
Test_C4	119.0 ± 0.7	199.3 ± 2.2	59.6 ± 1.0	Test_C4	125.6 ± 1.1	211.5 ± 3.2	62.5 ± 1.4
ThinFilmVD (average)	**119.4 ± 0.6**	**200.5 ± 2.0**	**59.6 ± 0.9**	**ThinFilmVD** (average)	**125.6 ± 1.2**	**211.7 ± 3.4**	**62.5 ± 1.6**
Santos et al.[39]	119.0 ± 0.6	199.5 ± 1.6	59.5 ± 0.8	Ribeiro da Silva et al.[33]	125.6 ± 0.6	211.0 ± 2.0	62.7 ± 0.8
de Kruif[38]	119.5 ± 2.4	200.6	59.7	Ribeiro da Silva et al.[48]	124.5 ± 0.6	209.1 ± 1.5	62.2 ± 0.7
Roux/Temprado et al.[40]	120.1 ± 3.3			Ribeiro da Silva et al.[48]	128.0 ± 2.1		
Hoyer/Peperle[47]	120.6 ± 4.1			Santos et al.[31]	125.3 ± 1.1	211.1 ± 2.9	62.4 ± 1.4
				Burkinshaw/Mortimer[49]	121.8 ± 5.4		
	1,3,5-Triphenylbenzene				Perylene		
Test_C1	147.3 ± 1.3	250.6 ± 3.6	72.5 ± 1.7	Test_C1	135.6 ± 0.9	208.5 ± 2.3	73.4 ± 1.1
Test_C2	148.4 ± 1.4	253.4 ± 3.6	72.8 ± 1.7	Test_C2	135.6 ± 0.9	209.4 ± 2.4	73.2 ± 1.2
Test_C3	149.2 ± 1.2	255.3 ± 3.4	73.1 ± 1.6	Test_C3	135.9 ± 1.0	210.0 ± 2.4	73.3 ± 1.2
Test_C4	148.4 ± 1.3	253.3 ± 3.4	72.8 ± 1.6	Test_C4	136.4 ± 0.9	209.9 ± 2.3	73.8 ± 1.1
ThinFilmVD (average)	**148.3 ± 1.3**	**253.2 ± 3.5**	**72.8 ± 1.7**	**ThinFilmVD** (average)	**135.8 ± 0.9**	**209.4 ± 2.3**	**73.4 ± 1.2**
Ribeiro da Silva et al.[33]	145.7 ± 1.2	247.6 ± 3.4	71.9 ± 1.6	Santos et al.[31]	133.2 ± 0.6	203.3 ± 1.5	72.6 ± 0.7
Santos et al.[31]	148.4 ± 1.0	253.4 ± 2.8	72.8 ± 1.3	Goldfarb et al.[53]	131.0 ± 2.3		
Verevkin[50]	145.8 ± 1.1	255.5 ± 3.0	72.3 ± 1.4	Oja et al.[54]	137.2 ± 4.5		
Malaspina et al.[51]	146.8 ± 1.8	247.3 ± 4.5	73.1 ± 2.2	Inokuchi et al.[55]	134.6 ± 5.4		
Wakayama/Inokuchi[52]	146.8 ± 0.9	245.6 ± 2.5	73.6 ± 1.2				
Hoyer/Peperle[47]	146.8 ± 0.7	249.4 ± 2.1	72.4 ± 0.9				

[a]The uncertainties (twice the deviation of the mean) of the thermodynamic properties of sublimation at T = 298.15 K were calculated by using the rules of propagation of uncertainty.